Improving NOAA 20 VIIRS Screen Transmittance and Solar Diffuser BRF estimation from Yaw maneuver and Regular On-orbit data

Taeyoung Choi[1,2*], Slawomir Blonski[1,2], Xi Shao[3,2], Changyong Cao[2]

[1]Earth Resources Tech. Inc. 14401 Sweitzer Lane Suite 300 Laurel, MD 20707 U.S.A
[2]NOAA Center for Satellite Applications and Research (STAR) 5830 University Research Ct. College Park MD 20740-3818, U.S.A.
[3]University of Maryland, College Park MD 20707 U.S.A

ABSTRACT

The Visible Infrared Imaging Radiometer Suite (VIIRS) aboard the NOAA 20 satellite performs radiometric calibration based on the Solar Diffuser (SD) collections for the Reflective Solar Bands (RSBs). The SD Bidirectional Reflectance Function (BRF) degradation (or H-factor) is measured by the Solar Diffuser Stability Monitor (SDSM) which uses Digital Count (DC) ratios between the signals of sunlit to SD and direct Sun illumination through a pinhole screen. The H-factor trends derived using the prelaunch version of the Sun view SDSM transmittance LUT show abnormal oscillations. This problem was not resolved even after applying the updated LUTs from the yaw maneuvers conducted on January 25th and 26th, 2018.

As an alternative approach, the NOAA VIIRS team developed a methodology to update the noisy SDSM Sun transmittance function from the regular on-orbit SDSM collections. Initially, the on-orbit SDSM collections were performed each time VIIRS was approaching the night-to-day terminator. The frequency of SDSM collects was reduced to every other orbit starting from Dec. 14th, 2017. It was further reduced to once per day starting from Jan. 5th, 2018. From all the on-orbit SDSM collects, the SDSM Sun view transmittance function is calculated from the DC of the SDSM sun view at the time of SDSM collection, time dependent gain changes of the 8 SDSM detectors, incident Sun angle, Earth-satellite distance and solid angle of the SDSM Sun view. A new Sun transmittance LUT is derived using a combined data set from the yaw maneuver data and the on-orbit SDSM collection data with SDSM detector degradation correction. The new LUT significantly reduces uncertainties of SD degradation estimates (H-factor) from 0.8 percent to 0.2 percent level. Further improvements will be performed once a one-year cycle of SDSM solar azimuth changes will be completed.

Keywords: NOAA 20, VIIRS, RSB, Yaw Maneuver, Solar Diffuser, Solar Diffuser Stability Monitor, SD, SDSM

1. INTRODUCTION

On November 18th, 2017, the Visible Infrared Imaging Radiometer Suite (VIIRS) on Joint Polar Satellite System 1 (JPSS1) / NOAA 20 (N20) satellite was launched. N20 VIIRS has 22 spectral bands that are composed of 14 Reflective Solar Bands (RSB), 7 Thermal Emissive Bands (TEB) and 1 Day-Night-Band (DNB) with a wide spectrum range of 0.412 μm to 12.5 μm. VIIRS is a scanning radiometer spatially covering a wide swath range of 3000 km in different nadir spatial resolutions of 375 and 750 m for imaging bands (I band) and moderate resolution bands (M bands). The N20 VIIRS was activated on November 19th and it started collecting the full-aperture Solar Diffuser (SD) observations along with the Solar Diffuser Stability Monitor (SDSM) data to monitor the SD degradation over time at 8 different wavelengths [1]. The 14 VIIRS RSBs are calibrated approximately 14 or 15 times per day by the solar light passing through a Solar Attenuation Screen (SAS). The attenuated sun light is reflected off the SD which is the primary source of RSB calibration as shown in Figure 1. For accurate RSB Sensor Data Record (SDR) production, the VIIRS calibration is dependent on the on-board SD and Space View (SV) digital number (DN) differences to determine the reflectance of the SD. One challenging and known property of the SD made of the Spectralon™ is that its reflectance gets gradually reduced by the exposure to strong space radiation such as solar Ultra Violet (UV) light and energetic particles[2][3]. The

Sensors, Systems, and Next-Generation Satellites XXII, edited by Steven P. Neeck, Philippe Martimort, Toshiyoshi Kimura, Proc. of SPIE Vol. 10785, 1078516 · © 2018 SPIE · CCC code: 0277-786X/18/$18 · doi: 10.1117/12.2324335

SDSM monitors the SD degradation by taking the ratio between the simultaneous measurements of Sun illumination transmitted by the SAS and the solar reflectance off the SD after passing through another SAS.

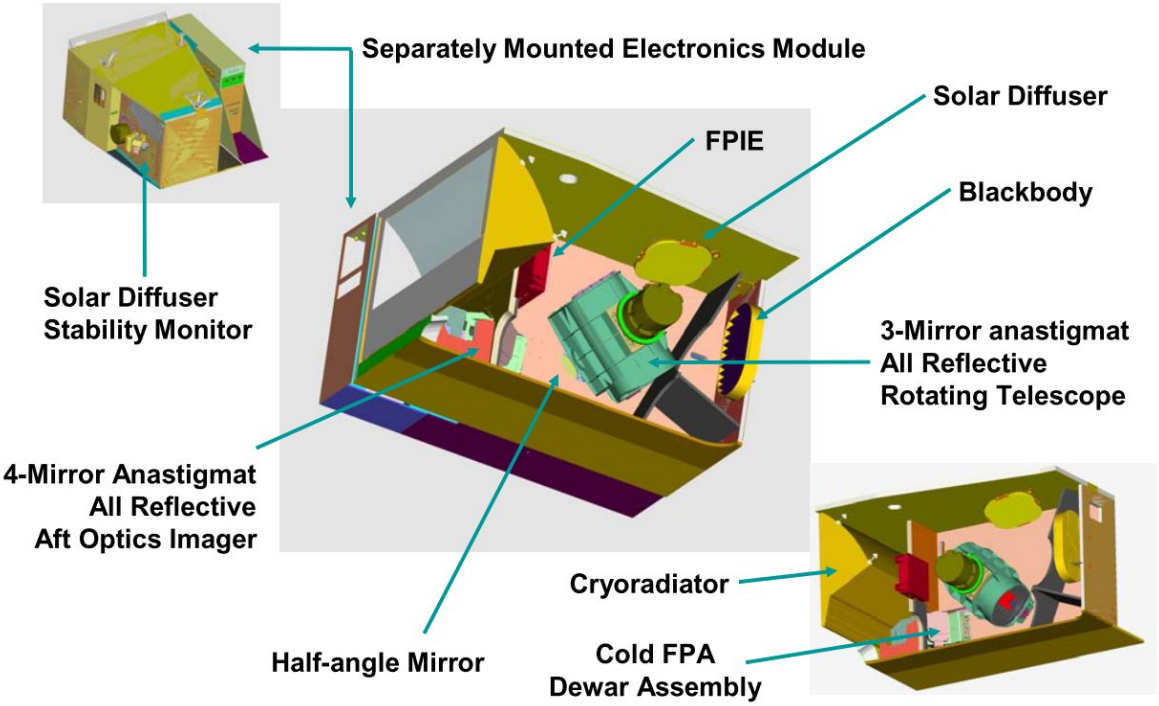

Figure 1. VIIRS Opto-Mechanical Module and on-board calibrators schematic [4].

The SD degradation (or H-factor) was calculated from the on-orbit SDSM measurements starting from the VIIRS activation on November 29, 2017. The initial SD degradation showed large fluctuations especially with the SDSM detector 8 which showed more than 1 percent changes within 70 Days Since Launch (DSL) [1]. These large oscillations in the H-factor indicated that there were potential problems with the prelaunch SDSM SD view BRF LUT and SDSM Sun view transmittance LUT. With these LUTs updated based on the N20 VIIRS 15 yaw maneuvers conducted on January 25 to 26, 2018, the H-factor responses showed expected wavelength dependency, and the large oscillations were reduced for all SDSM detectors. These results also proved that the prelaunch SDSM LUTs were not applicable for the correct screen transmittance or SD BRDF function.

In this study, detailed descriptions of the on-orbit yaw maneuvers and derivation procedures of SDSM Sun screen transmittance function (τ_{SDSM}) and SD view transmittance function with BRDF to the SDSM SD view port ($\tau_{SD} \cdot BRDF_{SDSM}$) are provided to mitigate the H-factor oscillation problems. Following section 2 describes the on-orbit RSB calibration with the relationship between the H-factor and F-factor. In section 3, detailed descriptions of the yaw maneuvers and the derivation procedures of the three LUTs (τ_{SDSM}, $\tau_{SD} \cdot BRDF_{SDSM}$, and $\tau_{SD} \cdot BRDF_{SD}$) are provided. In result section (section 4), the updated H-factors using the yaw maneuver derived LUTs are compared to the initial version using the prelaunch LUTs. To improve the performance of on-orbit H-factor calculation, regular on-orbit SDSM data sets are merged to yaw maneuver data set. By combining the yaw and regular on-orbit SDSM data sets together, stable H-factor responses are calculated and applied to NOAA's VIIRS SDR production system. Section 5 provides the summary of this study.

2. ON-ORBIT RSB CALIBRATION

2.1 Regular on-orbit SDSM operations

On November 29 of 2017, the N20 VIIRS was activated and the SDSM started operation providing the Sun and SD view Digital Counts (DC) at the termination point near the South Pole with a frequency of 14 or 15 times per day. The SDSM was set to operate every orbit from the start of activation to December 8, 2018. Since there was no major problem in the SDSM operations, the frequency was reduced to every other orbit until January 5, 2018. The SDSM operation frequency was further reduced to once per day to save SDSM motor movements [1]. Figure 2 shows a diagram of VIIRS Rotating Telescope Assembly (RTA), SD, SDSM and screens. The reflectance of SD is supposed to be spectrally flat but it gets degraded by the Ultraviolet (UV) portion of the Sun illumination. The degradation is caused by the surface roughness which is way smaller than the wavelength with a relationship of the $1/\lambda^{-4}$ in the degradation pattern, which is called a Surface Roughness Rayleigh Scattering (SRRS) model [2]. The accurate estimation of this SD degradation is key for the successful VIIRS radiometric calibration in the RSBs.

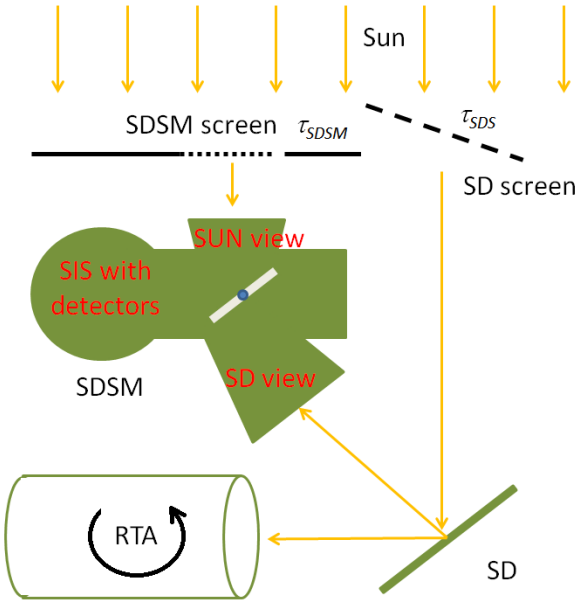

Figure 2. A simplified schematic of screens, SD, SDSM and RTA relations with illumination from the Sun.

2.2 SD Degradation (H-factor) Calculation

As shown in Figure 2, the SDSM includes an integrating sphere with 8 detectors at different wavelengths, Sun view port, SD view port, and a rotating mirror. There are three modes of Sun, SD, and dark views that are controlled by the step motor inside of the SDSM. When the solar illumination is within the desired angle range which is called 'sweet spot', the H-factor is calculated by Equation 1. The H-factor is basically a ratio between the DC values of SD and Sun with the screen transmittances, SD BRDF, and incident angle corrections. In following Equation 1, dc_{SD} is the bias removed SD view DC, τ_{SDSM} is the SDSM Sun screen transmittance, dc_{SUN} is the bias removed SDSM Sun view DC, τ_{SDS} is the SD screen transmittance function, BRF_{SDSM_SD} is the BRF at the SDSM viewing angle to the SD surface, and Ω_{SDSM} is the solid angle of the SDSM SD view port.

$$H(t) = \frac{dc_{SD} \cdot \tau_{SDSM}}{dc_{SUN} \cdot BRF_{SDSM\_SD} \cdot \tau_{SDS} \cdot \cos(\theta_{inc}) \cdot \Omega_{SDSM}} \qquad \text{Equation 1}$$

2.3 F-factor Calculation

The calibration source for the RSBs is the on-board SD. The BRF of SD is well known and measured in the prelaunch calibration with the National Institute of Standard Technology (NIST) back traceability. In Equation 2, the F-factors are calculated when the SD is in the 'Sweet Spot' angle ranges. The horizontal and vertical solar incoming incident angels on the SD surface changes the reflectance responses which is characterized by the BRF function. The H-factor modifies the time dependent SD degradation on top of the BRF function.

$$F = \frac{\mathrm{RVS}_{SD} \cdot \cos(\theta_{inc}) \cdot \left\{ E_{sun} \cdot \tau_{sd} \cdot \frac{H(t)}{H(t_0)} \cdot BRF_{Pre\_SD} \right\}}{C_0 + C_1 \cdot dn_{SD} + C_2 \cdot dn_{SD}^2 + C_3 \cdot dn_{SD}^3} \qquad \text{Equation 2}$$

In Equation 2, the RVS_{SD} is response versus scan at the SD angle, θ_{inc} is the Sun incident angle on the SD screen, E_{sun} is solar irradiance value within the VIIRS spectral band, τ_{sds} is the SD screen transmittance, $BRDF_{SD}$ is the SD BRDF that is modified by the H-factor, $C_{0,1,2}$ are electronics and detector temperature effect corrected prelaunch coefficients, and the dn_{SD} is bias removed SD digital number by the SV responses within the same scan.

3. YAW MANEUVERS AND DATA PROCESSING

3.1 Overview of the N20 VIIRS Yaw Maneuvers

Through January 25th to 26th, a series of scheduled yaw maneuvers was performed for the N20 spacecraft affecting all the on-board sensors. There were 15 yaw maneuvers are listed in table 1 with the spacecraft yaw angles, orbit numbers and time stamps. Similar to the S-NPP case, the spacecraft was in the desired yaw angle well before the center time of the SD observation time near the South Pole and returned to the normal operation angle for each yaw maneuver. The yaw angles were selected and simulated to cover slightly beyond the yearly variation range for the SD and SDSM solar azimuth angles.

Table 1.N20 yaw maneuver information.

#	date	Time [UTC]	Orbit #	Yaw angle
1	1/25/2018	21:07	972	-7.272
2	1/25/2018	22:48	973	-6.034
3	1/26/2018	00:30	974	-4.793
4	1/26/2018	02:11	975	-3.555
5	1/26/2018	03:53	976	-2.316
6	1/26/2018	05:34	977	-1.076
7	1/26/2018	07:16	978	0.162
8	1/26/2018	08:57	979	1.401
9	1/26/2018	10:39	980	2.640
10	1/26/2018	12:20	981	3.880
11	1/26/2018	14:02	982	5.119
12	1/26/2018	15:43	983	6.358
13	1/26/2018	17:25	984	7.596
14	1/26/2018	19:06	985	8.836
15	1/26/2018	20:48	986	10.075

3.2 VIIRS SD Screen Transmittance and BRF Function Derivation (τ_{SD}·BRF)

From the F-factor equation (Equation 2), the combined SD screen transmittance and SD BRF function can be derived by reorganizing the equation. Since the RTA view SD Reponses already include the screen transmission and SD reflected BRF function, the τ_{SD}·BRF was treated as one response in Equation 3.

$$\tau_{SD} \cdot BRF = \frac{F(t_{yaw})\cdot[C_0+C_1\cdot dn_{SD}+C_2\cdot dn_{SD}^2]}{\cos(\theta_{inc})\cdot E_{Sun}\cdot H(t_{yaw})\cdot RVS_{SD}} \quad \text{Equation 3}$$

In each VIIRS detector, gain, HAM side and scan in the On Board Calibration Intermediate Product (OBCIP) files during the yaw maneuvers and the C coefficients, F-factors, and H-factors were interpolated to get the τ_{SD}·BRF value along with the SD declination and azimuth angles.

3.3 SDSM Sun Screen Transmittance Function (τ_{SDSM})

This function can be derived from the H-factor equation (Equation 1). In the SDSM Sun screen transmittance function in following Equation 4, it should be noted that the representative time of yaw maneuver (t_{yaw}) is fixed at the middle time of the all the yaw maneuvers.

$$\tau_{SDSM} = \frac{H(t_{yaw})\cdot dc_{SD}\cdot\tau_{SD}\cdot BRDF_{SDSM}\cdot dc_{Sun}\cdot\cos\,\theta_{inc}\cdot sin^2\varphi}{\tau_{SD}} \quad \text{Equation 4}$$

3.4 SDSM SD Screen Transmittance and SDSM BRF Function (τ_{SD}·BRF_{SDSM})

The SDSM detector gain through SD view can defined in Equation 5.

$$G_{SDSM\_SD\_view} = \frac{\tau_{SD}\cdot BRF_{SDSM}\cdot\cos(\theta_{SD})\cdot H(t_{yaw})\cdot E_{Sun}\cdot sin^2\varphi}{dc_{SD}} \quad \text{Equation 5}$$

The numerator of the Equation 5 represents the Sun irradiance incident on the SDSM detector through SD view and the denominator which is offset removed SDSM detector SD response in the Digital Count (DC). Since it was measured at the time of yaw maneuver, the H-factor time was fixed in the middle of yaw maneuver time. The τ_{SD}·BRF_{SDSM} was measured by using Equation 6. The details of the gain derivation was well described in the McIntire's work [5].

$$\tau_{SD} \cdot BRF_{SDSM} = \frac{G_{SDSM\_SD\_view}\cdot dc_{SD}}{\cos(\theta_{inc})\cdot E_{Sun}\cdot sin^2\varphi} \quad \text{Equation 6}$$

The measurements performed and saved the information in each SDSM detector and scan within the sweet spot ranges with the SDSM elevation and azimuth angles.

4. RESULTS

4.1 Initial H-factor problems using prelaunch LUTs

Since the F-factor is dependent on the H-factor as shown Equation 2, the H-factors need to be calculate first. The initial N20 VIIRS H-factor was calculated from Equation 1 using the on-orbit SDSM collections. As shown in Figure 3, the H-factor was normalized by the value of the first SDSM measurement on orbit. The frequency of SDSM collections was initially once per orbit. On 12/8/2017 (Days Since Launch (DSL) 20), the frequency was reduced to every other orbit and it was further reduced to once per day since 1/5/2018 [1]. All the RSB related key events during the Post Launch Testing (PLT) period was listed in previous work [1]. The N20 H-factors in all the detectors showed very large oscillations up to 1.5 percent especially with the detector 8, when the degradation patterns were compared with the monotonically decreasing S-NPP case. When the Prelaunch SDSM Sun transmittance function was tested in Figure 4, the factor includes too much variations in time, which indicated potential problems with the prelaunch version of the τ_{SDSM}.

4.2 Initial yaw maneuver data processing and LUT derivation results

4.2.1 VIIRS SD Screen Transmittance and BRF Function (τ_{SD}·*BRF*) Results

The OBCIP files from the 15 yaw maneuvers listed in table 1 provided different levels of solar azimuth angles with continuous solar elevation angles for SDSM calibration or solar declination angles for SD calibration. Figure 5 (a) shows the Azimuth angle changes with the 15 yaw maneuvers and the red text indicates the individual orbit numbers (see Table 1). The SD declination angle range was roughly within 12 to 19 degrees. Each asterisk represents the yaw data point which was collected at each rotation of the RTA view to the SD. The high gain responses were used in the function estimation.

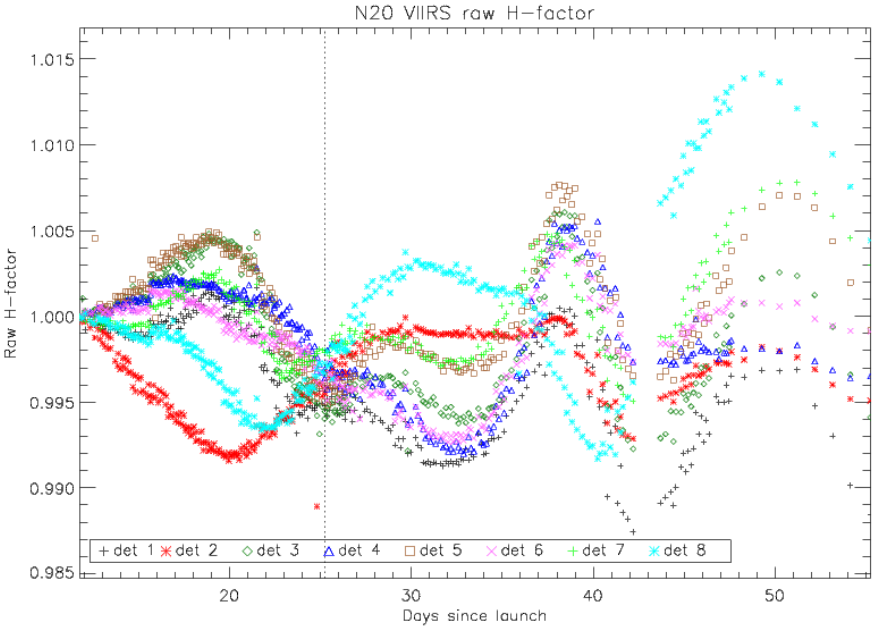

Figure 3. N20 VIIRS initial raw H-factor normalized to the first SDSM data point.

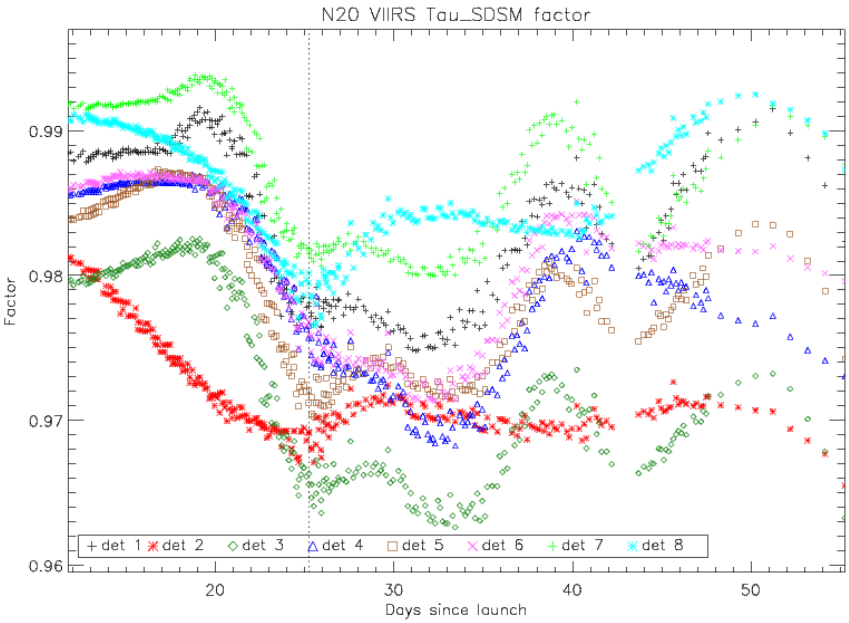

Figure 4. Prelaunch SDSM Sun transmittance function (τ_{SDSM})

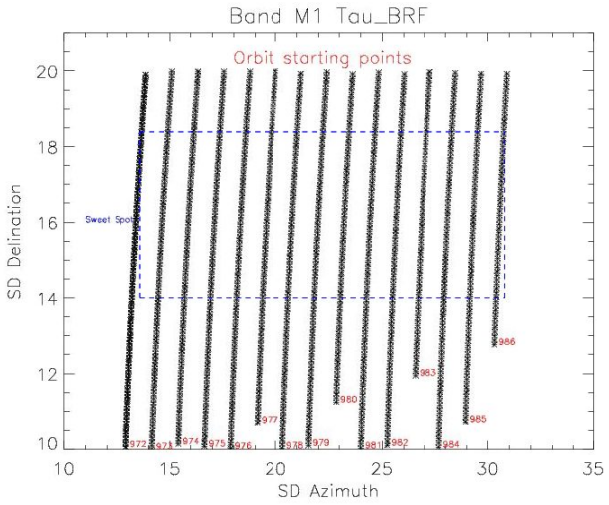

(a) RTA SD view (τ_{SD} BRF) data point locations

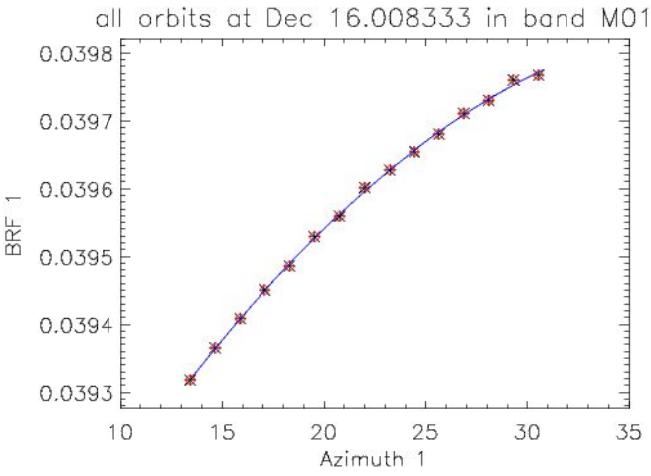

(b) Quadratic function fit at declination angle 16 degrees

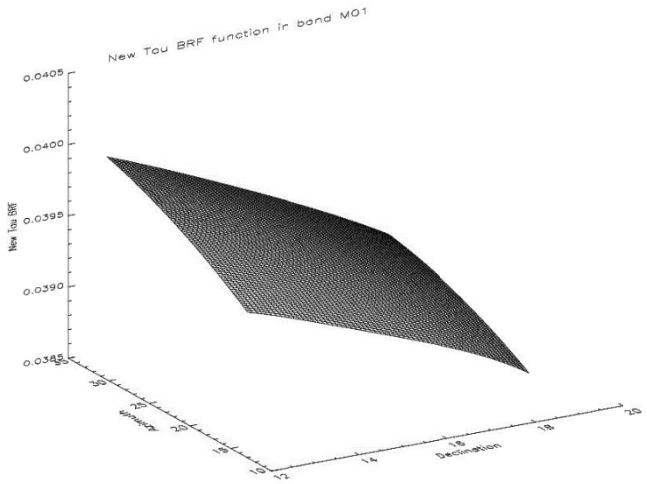

(c) New M1 1 τ_{SD} BRF function 3D plot

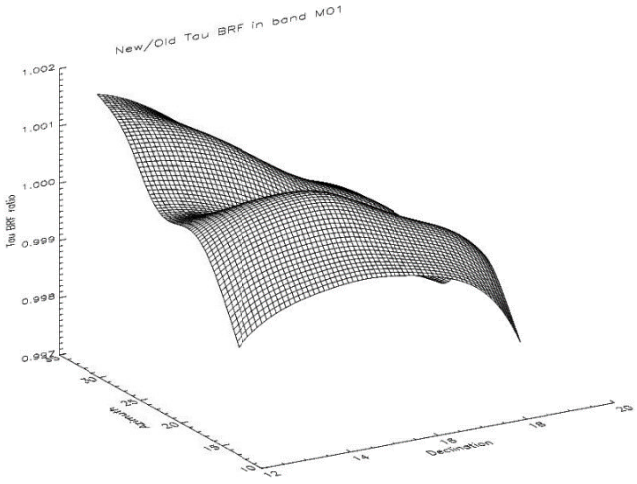

(d) Ratio between new and old (pre-launch) τ_{SD} BRF function

Figure 5. SD screen transmittance and BRF (τ_{SD} BRF) function derivation from the yaw maneuvers.

The current SD sweet spot definition is defined in the LUT called 'VIIRS-RSBAUTOCAL-H-LUT.' To be a valid SD observation for H-factor calculation, the SD declination angle should be greater than 14 degrees and less than 18.3916 degrees and the SD azimuth angle should be greater than 13.6 degrees and less than 30.78 degrees. To cover the sweet spot, the yaw maneuvers were carefully scheduled and performed as shown in Figure 5 (a). A quadratic function was fitted in each sub sample location of the declination angle as shown in Figure 5(b). With all the asterisk points in the Figure 5 (c), a new τ_{SD} BRF was interpolated in a smooth surface. When the new τ_{SD} BRF was compared with the pre-launch version, they were very similar surfaces within ±0.2 percent levels in Figure 5(d). The differences between the yaw data derived and pre-launch τ_{SD} BRF were very small. The difference plots in all other RSB bands had similar shapes and levels of differences; however, the yaw derived τ_{SD} BRFs were used when the F-factors were calculated.

4.2.2 SD Screen Transmittance and SDSM BRF Function ($\tau_{SD} \cdot BRF_{SDSM}$) Results

Before the F-factor updates, the H-factor related SDSM LUTs need to be correctly derived. The $\tau_{SD} \cdot BRF_{SDSM}$ was derived for all the 8 SDSM detectors at different wavelengths. The data locations in Figure 6 (a) are exactly the same as Figure 5 (a), since the solar attenuation screen is the same. Predominately, the $\tau_{SD} \cdot BRF_{SDSM}$ was decreasing along with the solar azimuth angle increase as shown in Figure 6 (b) and (c). Basically, there were small slopes in the ratio plot

between the yaw derived and pre-launch version of the SDSM detector 1 $\tau_{SD} \cdot BRF_{SDSM}$ from Figure 6 (d). Compared to the pre-launch version, the new $\tau_{SD} \cdot BRF_{SDSM}$ values were increased up to 0.4% near the corner of 12 degrees in solar declination angle and 30 degrees in solar azimuth angle. On the other hand, the ratio was decreasing -0.2 % near the other diagonal corner with 18 degrees in solar declination and 14 degrees in solar azimuth angle. The newly calculated $\tau_{SD} \cdot BRF_{SDSM}$ will correct up to 0.6% annual oscillations if this estimation was correctly derived compared to the pre-launch LUT.

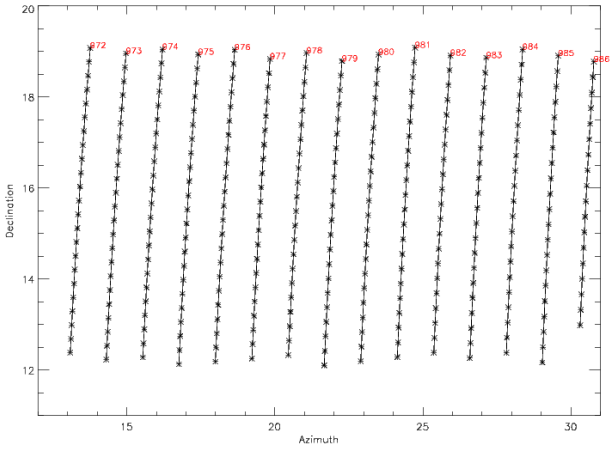

(a) SDSM SD view (τ_{SD} BRF) data point locations

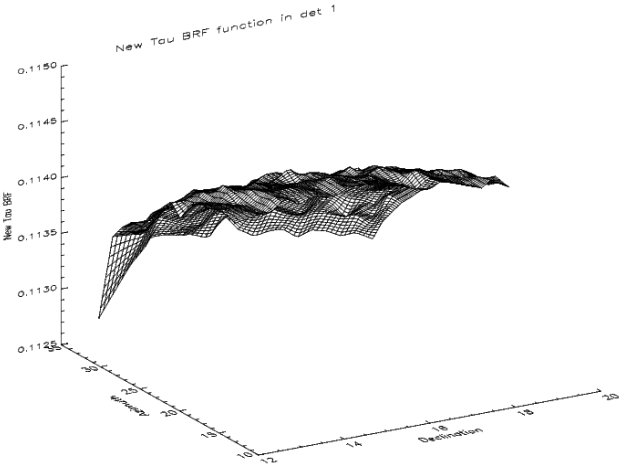

(b) SDSM detector 1 τ_{SD} BRF_{SDSM} function 3D plot

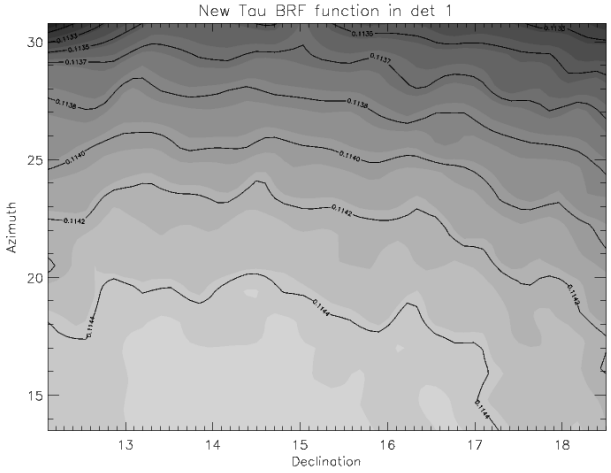

(c) SDSM detector 1 τ_{SD} BRF_{SDSM} function 3D plot

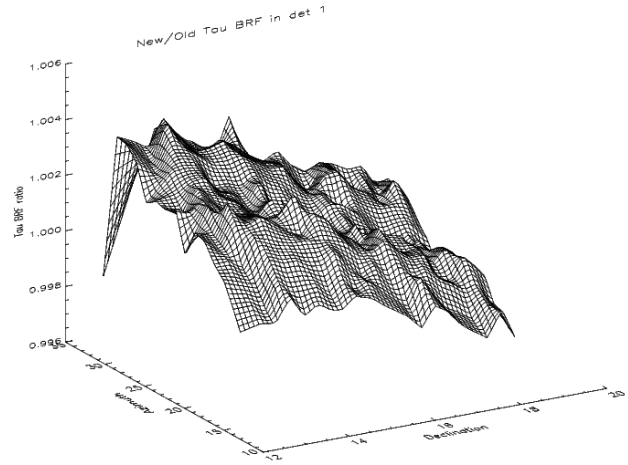

(d) Ratio between new and old τ_{SD} BRF_{SDSM} function

Figure 6. Combined SD screen transmittance and SDSM SD view BRF (τ_{SD} BRF_{SDSM}) function derivation plot.

4.2.3 SDSM Sun Screen Transmittance Function (τ_{SDSM}) Results

When the τ_{SDSM} were derived for each SDSM detector, it was resampled to a uniformly sampled grid space with the sampling step of 0.1 degrees with elevation and 0.21 degrees with azimuth angle. The elevation angle range was set to be from -2 degrees to 1.9 degrees, whereas the azimuth angle range was from -15 to 1.7875 degrees. This grid space for SDSM elevation and azimuth angles were determined when the J1 VIIRS pre-launch LUTs were built. Initially, it was assumed that this grid space was sufficient to represent right τ_{SDSM}. The SDSM detector 1 τ_{SDSM} yaw derived plots are

shown in Figure 7. As shown in Figure 7 (b) and (c), there were noticeably different between the two 3D surface shapes that were also reflected in the ratio plot in Figure 7 (d). The prelaunch version surface shape had detailed features,

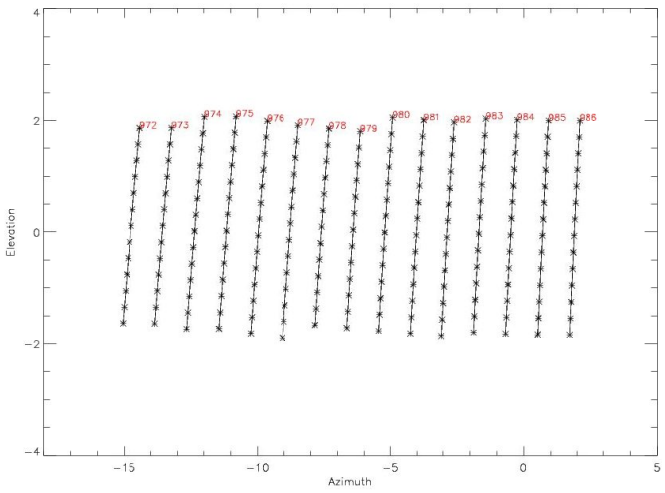

(a) SDSM Sun view τ_{SDSM} data point locations

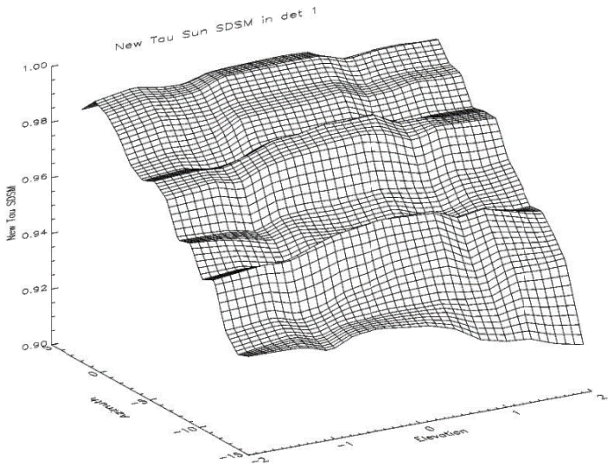

(b) Yaw derived SDSM D1 τ_{SDSM} 3D plot

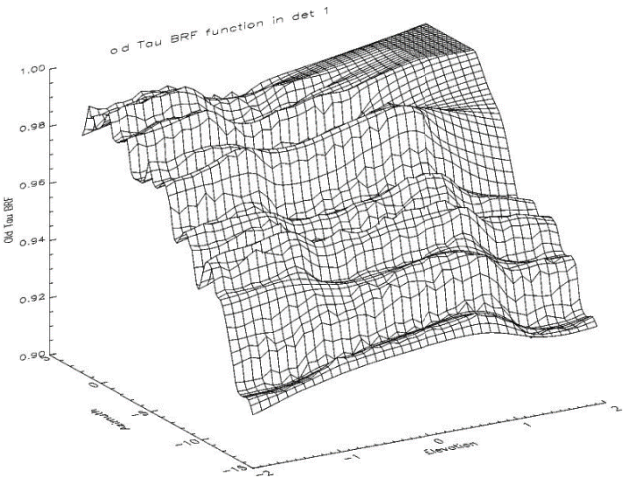

(c) Pre-launch SDSM D1 τ_{SDSM} 3D plot

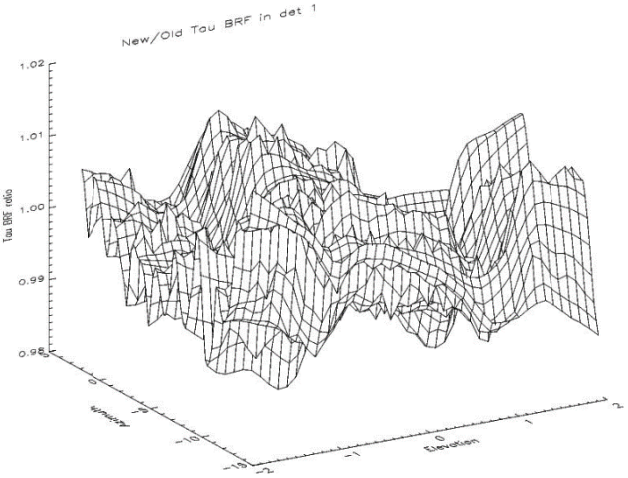

(d) Ratio between yaw derived and prelaunch τ_{SDSM}

Figure 7. SDSM Sun screen transmittance (τ_{SDSM}) function derivation plot.

whereas the yaw derived function was coarser than pre-launch version. The pre-launch τ_{SDSM} 3D plot in Figure 7 (c) showed a saturated plateau near the corner of the solar elevation angle 2 degrees and azimuth angle 5 degrees, but the yaw derived surface didn't show similar saturation point. The majority responses of the τ_{SDSM} function were similar that the yaw derived and pre-launch version values were increasing with the solar azimuth angle, while distinctive higher frequency ridge lines were observed in the pre-launch version. Because of these larger difference in the τ_{SDSM} function than other SDSM and SD BRF results, the ratio differences were approximately within ±1 percent level.

4.2.4 H-factor update with initial yaw maneuver data

To calculate an updated H-factor, the yaw maneuver derived τ_{SDSM} and τ_{SD} $\mathrm{BRF}_{\mathrm{SDSM}}$ functions were applied to the H-factor calculation using Equation 1. In each SDSM detector, H-factor response was normalized to the first day of the SDSM collection along with the N20 VIIRS activation date on November 29, 2017. All the updated H-factors are over

plotted in Figure 8. Compared to the H-factors with pre-launch LUTs in Figure 3, the yaw maneuver updated H-factors restored the frequency dependent SD degradation. The shortest wavelength SDSM detector 1 showed about 2 % degradation on yaw maneuver day at DSL 69, whereas the SDSM detector 8 showed 0.2 % degradation. On top of these wavelength dependency, the updated H-factor still had stability issues as shown 1 % level oscillations in Figure 8. As mentioned in previous study, the S-NPP VIIRS H-factors were stabilized showing very clean degradation pattern [1]. Clean initial H-factor trends were needed to extrapolate to the orbit insertion time and normalized as shown in Figure 9 at zero DSL point. In each SDSM detector, a linear exponential function fit was performed on the SDSM data set after the nadir open date (12/13/2017). Since the uncertainty level of the H-factor was too large (>1%), the linear exponential function fit was also unreliable. As result of it, the H-factor normalization points were not reliable nor applicable to calculate F-factors.

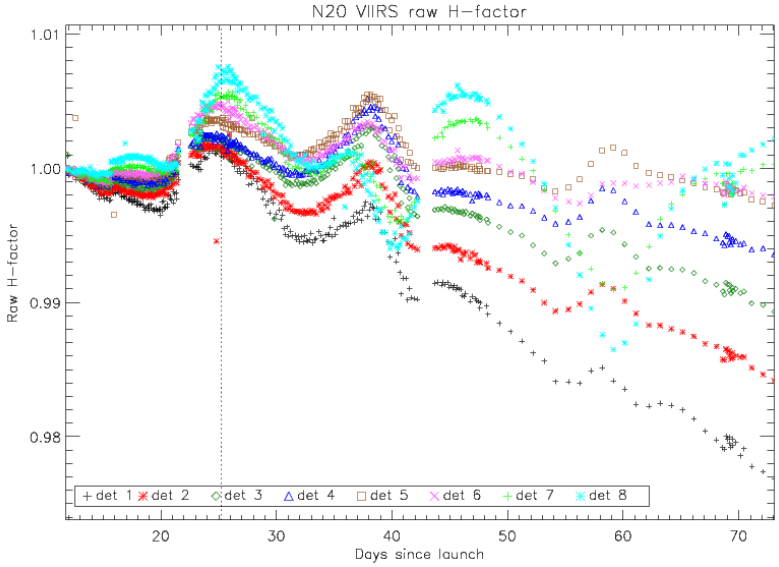

Figure 8. Raw H-factors after the yaw maneuver derived LUTs update (normalized to the first SDSM point).

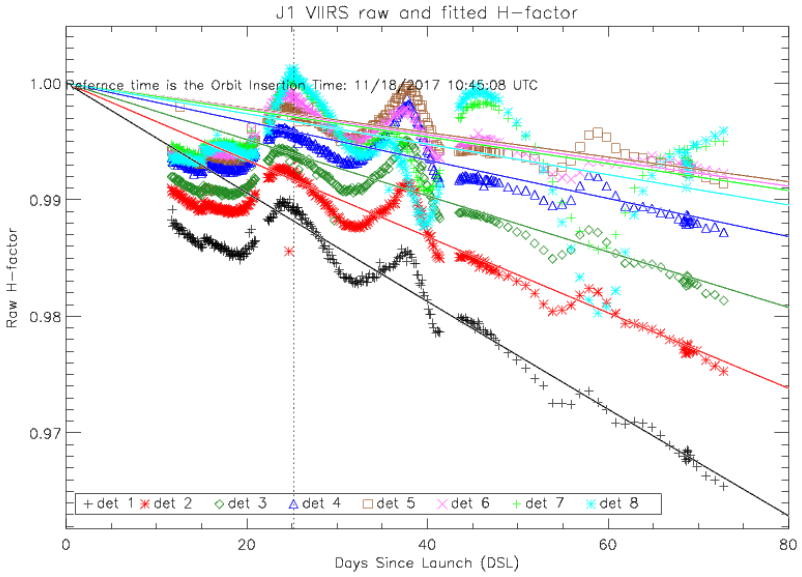

Figure 9. H-factor after the yaw maneuver derived LUTs update (normalized to the zero DSL point).

4.3 H-factor update with on-orbit SDSM data

When the H-factor related τ_{SDSM} and τ_{SD} $\mathrm{BRF}_{\mathrm{SDSM}}$ were checked, the τ_{SDSM} ratio differences to the pre-launch values were ±1 percent level. Therefore, the yaw updated H-factor oscillations were caused by the imperfect τ_{SDSM} values. When the yaw updated and pre-launch 3D plot surfaces were compared in Figure 7 (b) and (c), the yaw update surface showed less micro features than the pre-launch version especially in the azimuth direction. It was assumed that the 15 yaw maneuver angles listed in Table 1 were not enough to follow high variability in the τ_{SDSM} surface especially in the azimuth direction. To resolve this issue, the regular on-orbit SDSM collections were added to the yaw maneuver data. Figure 10 shows SDSM Sun azimuth angle changes from the start of VIIRS activation on 11/18/2017 to 2/6/2018 (DSL 80). The SDSM Sun screen solar azimuth angles started from -2 degrees and gradually decreased to -8 degrees by the DSL 80 in Figure 10. The effect of 15 yaw maneuvers are clearly seen as a vertical spread around DSL 68 to 69. The yaw maneuver data locations are shown as red lines and the on-orbit SDSM data locations are added as blue lines in Figure 11. Under an assumption that there was no SDSM detector response changes, the on-orbit SDSM data were added to the yaw maneuver data to derive the τ_{SDSM} surface. This updated τ_{SDSM} LUT was used for the H-factor calculation as shown in Figure 12.

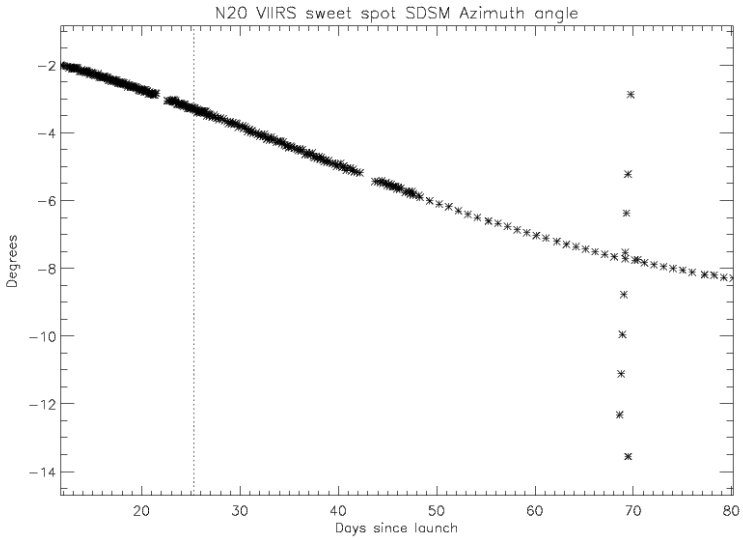

Figure 10. N20 VIIRS SDSM Sun screen solar azimuth angle in the middle of the 'sweet spot'.

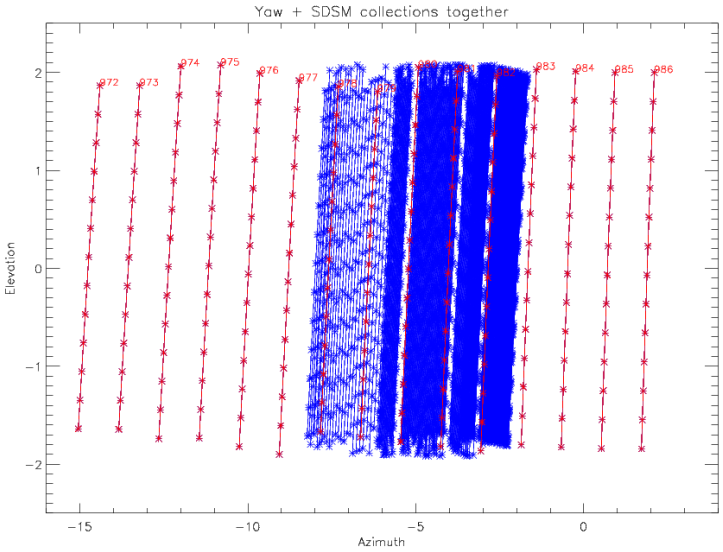

Figure 11. N20 VIIRS yaw maneuver and regular on-orbit SDSM data location in terms of SDSM Sun screen coordinates of solar elevation and azimuth angles.

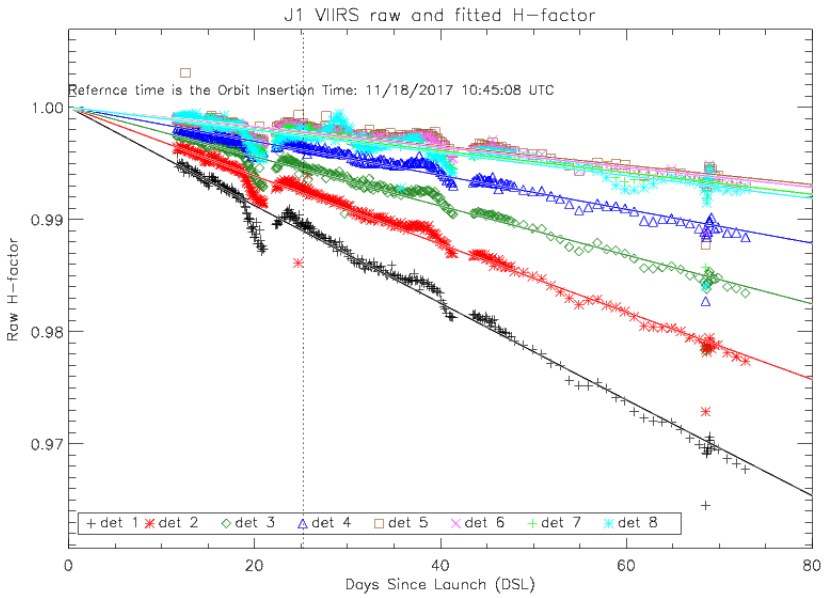

Figure 12. H-factor after the yaw and on-orbit SDSM data derived τ_{SDSM} LUT update.

The H-factors in Figure 12 significantly reduced the initial oscillation patterns. The stable H-factor played a very important role for the initial point extrapolation to find out initial point at the zero DSL. Compared to the H-factor fit in Figure 9, the yaw and on-orbit SDSM data derived H-factor provided higher confidence.

4.4 H-factor update with SDSM detector gain correction

In Figure 12, the yaw and on-orbit SDSM detector 6, 7 and 8 H-factors showed too much SD degradation compared to the S-NPP H-factors with the SDSM detectors [6]. Especially for SDSM detector 7 and 8 at wavelengths of 865 and 926nm, one percent degradation was achieved around 5 the year of operation with S-NPP case, but current version showed 0.7 percent degradation within 100 days of operation in Figure 12. To check any discrepancies, the yaw maneuver and on-orbit SDSM data values were visualized at the solar elevation angle of 0.8 degrees with the SDSM detector 8 in Figure 13.

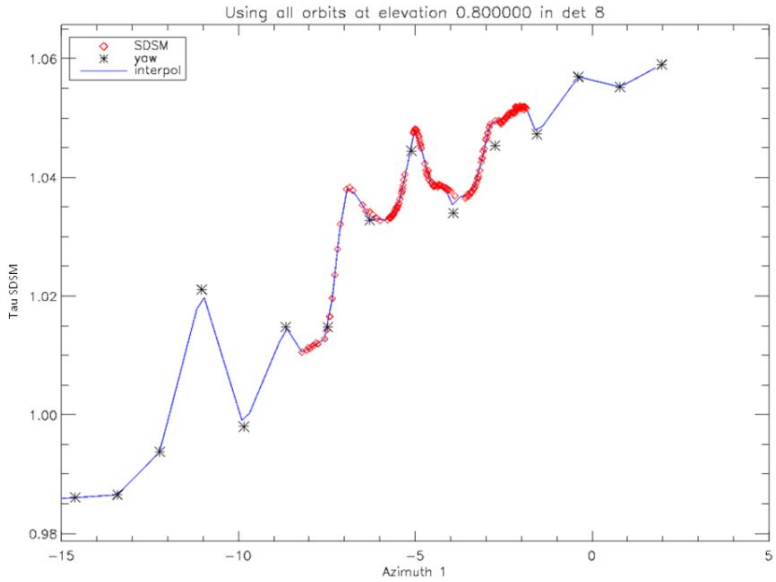

Figure 13. The yaw and on-orbit SDSM data over plot derived τSDSM LUT update

As expected, the on-orbit SDSM data points (red diamonds) provided fine structures in between the yaw data points (black asterisk) successfully; however, there was a tendency that the differences between the yaw and on-orbit SDSM data were increased from the solar azimuth angles from -7 to -2 degrees. Initially, it was assumed that there were no gain changes with the SDSM detectors but these differences indicated that gains must be handled correctly. When the interpolated on-orbit data points were divided by the yaw data, it showed a linear increase over the SDSM solar azimuth angle in Figure 14.

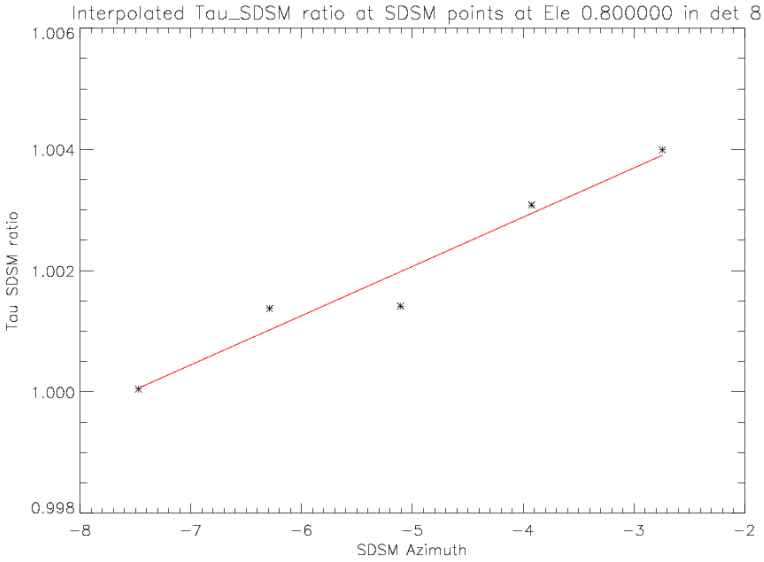

Figure 14. Interpolated on-orbit SDSM based τ_{SDSM} ratios at yaw maneuver data points.

The first point in Figure 14 is located at the SDSM azimuth angle near -7.5 degrees because the yaw maneuvers were performed very close to the on-orbit SDSM data. At this point, there was no large SDSM gain difference. When the yaw data was compared to the first on-orbit SDSM data near -2.5 degrees, there was more than 2 months' time difference so that the SDSM gain differences were large (~0.4%). The time dependency of the SDSM detector gains were linearly corrected along with the SDSM azimuth angle in all elevation angles as shown in Figure 15.

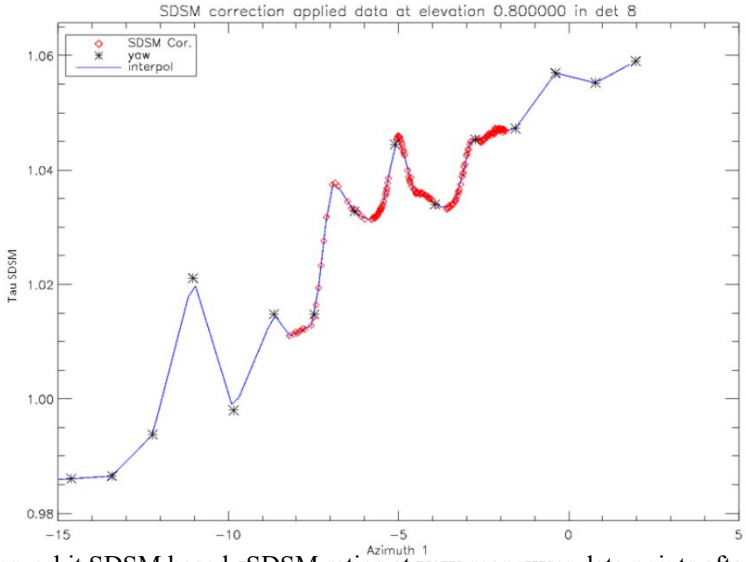

Figure 15. Interpolated on-orbit SDSM based τSDSM ratios at yaw maneuver data points after the SDSM gain correction.

In Figure 15, the on-orbit SDSM data points were aligned with the yaw maneuver points after the SDSM gain correction. Based on this results, the H-factors were updated as shown in Figure 16. In this H-factor, only the τ_{SDSM} LUT was replaced and reprocessed the entire H-factors. With the SDSM detector correction in the τ_{SDSM} LUT, the H-factor in Figure 16 was significantly improved with the abnormal detector 6, 7, and 8 degradation and oscillations near DSL 20 and 40 in the previous version of H-factor in Figure 12.

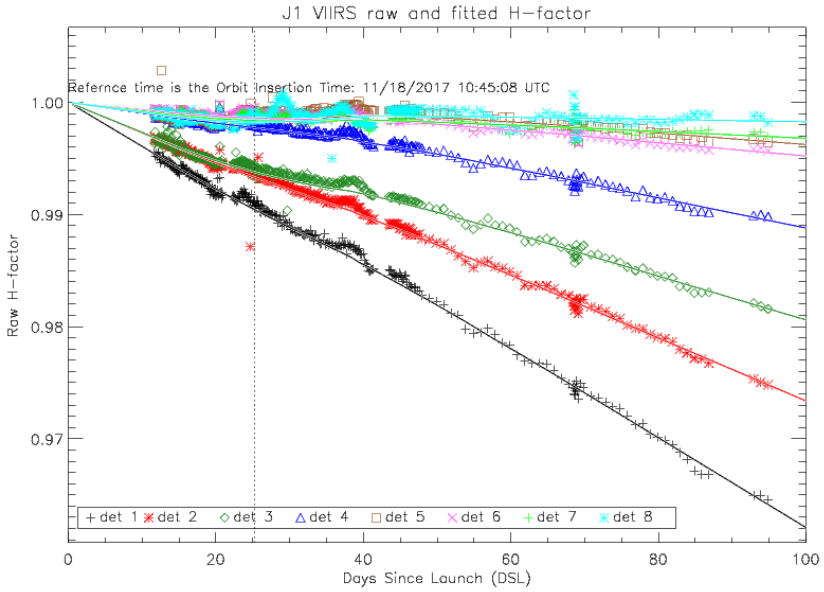

Figure 16. H-factor after the τ_{SDSM} LUT update with SDSM detector gain correction.

4.5 SD F-factor Result

When the H-factor issues were resolved, the F-factors were possibly calculated using Equation 2. Without getting stable H-factor, F-factor results were meaningless because they are linearly related as explained in Equation 2. The F-factors in Figure 16 were relatively stable when they were compared to the S-NPP F-factors especially in bands M5 to M10.

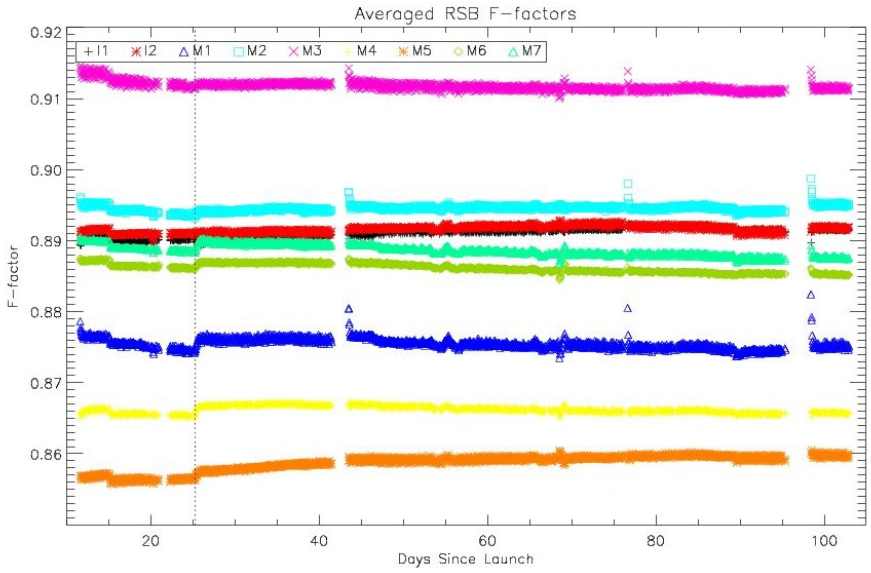

Figure 16. F-factor results after the H-factor update with SDSM detector gain correction.

Another concern was that the most N20 F-factors were way lower than S-NPP VIIRS case. These issues are currently under investigation along with the lunar F-factors, Deep Convective Cloud (DSS) trending, cross-calibration with other sensors such as Aqua MODIS and Landsat OLI sensors.

5. SUMMARY

For successful on-orbit radiometric calibrations of N20 VIIRS RSB, it is necessary to estimate accurate screen transmittance and BRF functions in the views of SDSM and VIIRS through RTA. Since these functions are the major sources of uncertainties, the yaw maneuver estimations are key for the calibration accuracy of the RSB under the situation that the H and F-factors are linearly related. The initial H-factor indicated that there were some problems with the pre-launch LUTs, because the H-factors showed abnormally large oscillations larger than 1 percent. To validate and resolve these issues, a series of 15 yaw maneuvers were performed in January of 2018. The resulting yaw-maneuver derived SD screen transmittance and BRF (τ_{SD} BRF) and SD screen and SDSM SD view BRF (τ_{SD} BRF_{SDSM}) provided reasonable agreements between the pre-launch and yaw results. When it comes to the SDSM Sun screen transmittance function (τ_{SDSM}), some issues found. First of all, there were significant ratio differences between the pre-launch and yaw derived version. Secondly, the yaw derived version didn't have fine features in the 3D surface in the solar azimuth direction. With the initial yaw LUTs, the H-factors restored the frequency dependent degradation but large peaks were appeared in all the SDSM detectors. Since the 15 yaw maneuver points were not able to follow the small features in the azimuth direction, on-orbit SDSM data sets were added for the τ_{SDSM} derivation. With this new τ_{SDSM} function, H-factors were reprocessed and the large oscillation patterns were mitigated; however, SDSM detectors 6, 7, and 8 showed abnormally high detector degradation compared to the S-NPP VIIRS case. The large SD degradations in the SDSM detectors 6, 7, and 8 were caused by the time dependent SDSM gain changes, whereas the yaw maneuvers were performed with in a day. The time dependent SDSM gain correction was applied with a ratio approach to match the on-orbit SDSM data and yaw maneuver point for the τ_{SDSM} function derivation. Finally reasonable H and F-factors were calculated with the final update of the τ_{SDSM} function. Compared to S-NPP VIIRS, N20 VIIRS F-factors showed very stable gain trends within 100 days of operation.

REFERENCES

[1] T. (Jason) Choi, S. Blonski, and C. Cao, "Initial on-orbit radiometric calibration of the NOAA 20 VIIRS reflective solar bands," in *SPIE Optical Engineering and Applications*, 2018.

[2] X. Shao, C. Cao, and T. C. Liu, "Spectral dependent degradation of the solar diffuser on Suomi-NPP VIIRS due to Surface Roughness-induced Rayleigh Scattering," *Remote Sens.*, vol. 8, no. 3, 2016.

[3] X. Xiong, A. Angal, T. Choi, J. Sun, and E. Johnson, "On-orbit performance of MODIS solar diffuser stability monitor," in *Proceedings of SPIE - The International Society for Optical Engineering*, 2012, vol. 8510.

[4] N. Baker, "Joint Polar Satellite System (JPSS) VIIRS Radiometric Calibration Algorithm Theoretical Basis Document (ATBD)," 2014.

[5] J. McIntire, D. Moyer, B. Efremova, H. Oudrari, and X. Xiong, "On-orbit characterization of S-NPP VIIRS transmission functions," *IEEE Trans. Geosci. Remote Sens.*, vol. 53, no. 5, pp. 2354–2365, 2015.

[6] T. Choi, X. Shao, C. Cao, and F. Weng, "Radiometric Stability Monitoring of the Suomi NPP Visible Infrared Imaging Radiometer Suite (VIIRS) Reflective Solar Bands Using the Moon," *Remote Sens.*, vol. 8, no. 1, p. 15, 2015.